

A JOINT LOOK ON LUNAR SATELLITE AND COOPERATIVE SURFACE PNT

Robert Pöhlmann, Emanuel Staudinger, Siwei Zhang, Armin Dammann

Institute of Communications and Navigation, German Aerospace Center (DLR)

ABSTRACT

A large number of missions to the Moon is planned in the coming years by both, public and private sectors. A high demand for a Lunar position, navigation and timing (PNT) system exists to aid landing, to support autonomous robotic exploration etc. ESA has proposed a satellite based system for communication and PNT. Furthermore, cooperative radio navigation for users on the Lunar surface, where PNT is provided through radio signals exchanged among robots and other entities, has been suggested. An analysis of the combination of satellite and cooperative navigation for Lunar PNT has not been done yet. In this paper, we provide a first estimation theoretic analysis of joint Lunar satellite and cooperative surface PNT. We derive the Bayesian Cramér-Rao bound (BCRB) and analyze the benefit of cooperation by comparing different cooperation strategies and scenarios, using system parameters from recent studies.

Index Terms— Bayesian Cramér-Rao Bound, Cooperation, Moon, Radio Navigation

1. INTRODUCTION

In the coming years, dozens of missions to the Moon are planned by both, public and private sectors [1]. Especially the Moon's south pole is a target of high interest due to the presence of water ice [2]. Communication and navigation plays a key role for the success of these missions, e.g. to aid landing and to support autonomous robotic exploration.

For past missions, navigation was provided by radiometric tracking from Earth, e.g. using NASA's deep space network (DSN), and laser tracking. While providing sufficient accuracy, independent tracking is costly and not suitable to continuously support a large number of missions. Furthermore, it is limited to the nearside of the Moon.

To meet the growing demand, ESA has proposed the Lunar Communication and Navigation Service (LCNS) as a solution that scales for a large number of users [3, 4]. A configuration of five satellites in elliptical Lunar frozen orbits (ELFOs) in three orbital planes has been suggested [4, 5], see Fig. 1. Lunar satellites shall provide means for communication and position, navigation and timing (PNT), where the PNT part is a one-way system heavily inspired by Earth global navigation satellite systems (GNSSs). LCNS

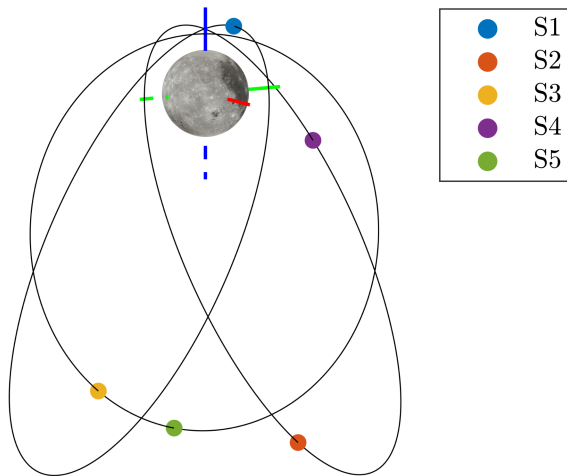


Fig. 1. Lunar satellite orbits suggested by [4, 5] in Moon centered inertial frame with x-, y- and z-axis in red, green and blue.

orbit determination and clock synchronization is foreseen to be accomplished using weak GNSS signals from Earth [6], to keep operational costs low. The achievable positioning performance using LCNS during landing has been analyzed in [4]. Navigation for a robotic surface mission, additionally using a digital elevation model (DEM) of the Moon, has been investigated in [7].

Cooperative radio navigation, also termed swarm navigation, has been suggested as a purely in-situ PNT system requiring no infrastructure [8]. All nodes in the network, e.g. a lander, robots and payload boxes with scientific instruments, exchange radio signals for communication and PNT. Extensive literature exists on algorithms and theory of cooperative navigation, see [9, 10] and the references therein. Recently, cooperative radio navigation has been demonstrated within a space-analogue mission [11].

An analysis of joint satellite and cooperative navigation for Lunar PNT has not been done yet. In this paper, we fill the gap by providing a performance analysis for combining Lunar satellite navigation and cooperative radio navigation among users on the Lunar surface. We derive the Bayesian Cramér-Rao bound (BCRB) for tracking as a lower bound on the mean squared error (MSE). We then analyze the benefit of cooperation by comparing physical and localization layer

cooperation, the cases of moving and static users and the dependency on the number of users.

2. STATE SPACE

2.1. State Definition

To tackle the problem, we define a state space for all unknown quantities. We distinguish between two different types of nodes listed in the set $\mathbb{N} = \{\mathbb{S}, \mathbb{U}\}$. First, satellites \mathbb{S} , which only transmit signals. Second, users \mathbb{U} , which receive signals from satellites and other users and transmit signals in broadcast mode. The state of user $i \in \mathbb{U}$ for epoch k is defined by

$$\mathbf{x}_i^k = [(\mathbf{p}_i^k)^T \quad (\mathbf{v}_i^k)^T \quad c\delta_i^k \quad c\dot{\delta}_i^k]^T, \quad (1)$$

with the three-dimensional user position \mathbf{p}_i^k and velocity \mathbf{v}_i^k . The clock offset δ_i^k and clock drift $\dot{\delta}_i^k$ are multiplied by the speed of light c . The full state

$$\mathbf{x}^k = [(\mathbf{x}_1^k)^T \quad \dots \quad (\mathbf{x}_i^k)^T \quad \dots \quad (\mathbf{x}_{|\mathbb{U}|}^k)^T]^T \quad (2)$$

is obtained by stacking the states of $|\mathbb{U}|$ users.

2.2. Process Model

The process model, describing the transition between epochs, is given by

$$\mathbf{x}^{k+1} = \mathbf{F}^{k+1}\mathbf{x}^k + \mathbf{w}^k. \quad (3)$$

The transition matrix

$$\mathbf{F}^{k+1} = \text{diag}\{\dots, \mathbf{F}_i^{k+1}, \dots\} \quad (4)$$

is block-diagonal, with the block corresponding to user i given by

$$\mathbf{F}_i^{k+1} = \begin{bmatrix} \mathbb{I}_3 & T\mathbb{I}_3 & \mathbf{0} & \mathbf{0} \\ \mathbf{0}_3 & \mathbb{I}_3 & \mathbf{0} & \mathbf{0} \\ \mathbf{0}^T & \mathbf{0}^T & 1 & T \\ \mathbf{0}^T & \mathbf{0}^T & 0 & 1 \end{bmatrix}, \quad (5)$$

where T is the time interval between epochs, \mathbb{I}_n is an identity matrix of dimension n and $\mathbf{0}$ an all-zero column vector. We use $\text{diag}\{\cdot\}$ as an operator that creates a square matrix from the elements or sub-matrices on the diagonal. A continuous white noise acceleration model [12] is assumed for the position and velocity states and a two-state clock model [13] for the clock states. The process noise

$$\mathbf{w}^k \sim \mathcal{N}(\mathbf{0}, \mathbf{Q}^k) \quad (6)$$

is Gaussian. The process noise covariance matrix

$$\mathbf{Q}^k = \text{diag}\{\dots, \mathbf{Q}_i^k, \dots\} \quad (7)$$

has a block-diagonal structure and is defined per user i ,

$$\mathbf{Q}_i^k = \begin{bmatrix} \frac{T^3\sigma_{i,v}^2}{3}\mathbb{I}_3 & \frac{T^2\sigma_{i,v}^2}{2}\mathbb{I}_3 & \mathbf{0} & \mathbf{0} \\ \frac{T^2\sigma_{i,v}^2}{2}\mathbb{I}_3 & T\sigma_{i,v}^2\mathbb{I}_3 & \mathbf{0} & \mathbf{0} \\ \mathbf{0}^T & \mathbf{0}^T & \sigma_{i,c1}^2T + \sigma_{i,c2}^2\frac{T^3}{3} & \sigma_{i,c2}^2\frac{T^2}{2} \\ \mathbf{0}^T & \mathbf{0}^T & \sigma_{i,c2}^2\frac{T^2}{2} & \sigma_{i,c2}^2T \end{bmatrix}. \quad (8)$$

with velocity noise coefficient $\sigma_{i,v}$ and clock noise coefficients $\sigma_{i,c1}$, $\sigma_{i,c2}$. For static users, the \mathbf{v}_i^k is omitted from the state vector and $\sigma_{i,v} = 0 \text{ m/s}^{1.5}$.

2.3. Observation Model

We consider pseudorange observations based on the signal delay and pseudorange rate observations based on the signal Doppler. The pseudorange for a signal transmitted by node $j \in \mathbb{N}$ and received by user $i \in \mathbb{U}$ at epoch k is given by

$$\rho_{i,j}^k = \|\mathbf{p}_j^k - \mathbf{p}_i^k\| + c\delta_j^k - c\delta_i^k + \epsilon_{i,j}^p, \quad (9)$$

with the noise

$$\epsilon_{i,j}^p \sim \mathcal{N}(\mathbf{0}, \sigma_{\rho_{i,j}^k}^2), \quad (10)$$

$$\sigma_{\rho_{i,j}^k} = \begin{cases} \sigma_{\mathbf{p}_j} + \sigma_{c\delta_j} + \sigma_{\text{DLL}} & j \in \mathbb{S} \\ \sigma_{\rho_u} & j \in \mathbb{U}. \end{cases} \quad (11)$$

The satellite position, velocity, clock offset and drift are broadcast via the ephemeris. The errors are mapped to the observations, also called signal-in-space error (SISE) in GNSS jargon, with $\sigma_{\mathbf{p}_j}$ and $\sigma_{c\delta_j}$ representing the satellite position error and clock error standard deviations, respectively. Furthermore, σ_{DLL} represents the delay-locked loop (DLL) noise and σ_{ρ_u} the ranging error standard deviation among users.

The pseudorange rate for a signal transmitted by node j and received by user i at epoch k is modeled as

$$\dot{\rho}_{i,j}^k = (\mathbf{v}_j^k - \mathbf{v}_i^k)^T \mathbf{u}_{i,j}^k + c\dot{\delta}_j^k - c\dot{\delta}_i^k + \epsilon_{i,j}^{\dot{\rho}}, \quad (12)$$

with the unit vector from user i to node j

$$\mathbf{u}_{i,j}^k = \frac{\mathbf{p}_j^k - \mathbf{p}_i^k}{\|\mathbf{p}_j^k - \mathbf{p}_i^k\|} \quad (13)$$

and the noise

$$\epsilon_{i,j}^{\dot{\rho}} \sim \mathcal{N}(\mathbf{0}, \sigma_{\dot{\rho}_{i,j}^k}^2), \quad (14)$$

$$\sigma_{\dot{\rho}_{i,j}^k} = \begin{cases} \sigma_{\mathbf{v}_j} + \sigma_{c\dot{\delta}_j} + \sigma_{\text{FLL}} & j \in \mathbb{S} \\ \sigma_{\dot{\rho}_u} & j \in \mathbb{U}. \end{cases} \quad (15)$$

Analog to (11), $\sigma_{\mathbf{v}_j}$ and $\sigma_{c\dot{\delta}_j}$ are the satellite velocity error and satellite clock drift error standard deviations, σ_{FLL} the frequency-locked loop (FLL) noise and $\sigma_{\dot{\rho}_u}$ the range rate error standard deviation among users.

To calculate the BCRB in the next section, we also need the Jacobian matrix \mathbf{H}^k representing the linearization of the

observation model about the state. Defining $l(i, j)$ as a function returning the index of the link between transmitting node j and receiving user i , \mathbf{H}^k consists of the blocks $\mathbf{H}_{l(i,j),i}^k$. The content of the blocks depends on the type of transmitting node and the cooperation mode. For physical layer cooperation, the local communication system is driven by the same oscillator as the satellite receiver. This allows to use pseudo-range and Doppler observations among users. Localization layer cooperation means nodes can observe noisy distances to their neighbors. This corresponds to the case, where the local communication and ranging is provided by a subsystem which is completely independent of the satellite receiver. The performance of the two cooperation modes is compared in Section 4.2. For $j \in \mathbb{S}$, or for $j \in \mathbb{U}$ if we consider physical layer cooperation among users, the blocks are defined by

$$\begin{aligned} \mathbf{H}_{l(i,j),i}^k &= -\mathbf{H}_{l(i,j),j}^k \\ &= \begin{bmatrix} -(\mathbf{u}_{i,j}^k)^T & \mathbf{0}^T & 1 & 0 \\ -(\mathbf{v}_{i,j}^k)^T & -(\mathbf{u}_{i,j}^k)^T & 0 & 1 \end{bmatrix}. \end{aligned} \quad (16)$$

For $j \in \mathbb{U}$ if we consider localization layer cooperation, the blocks are defined by

$$\begin{aligned} \mathbf{H}_{l(i,j),i}^k &= -\mathbf{H}_{l(i,j),j}^k \\ &= \begin{bmatrix} -(\mathbf{u}_{i,j}^k)^T & \mathbf{0}^T & 0 & 0 \\ \mathbf{0}^T & \mathbf{0}^T & 0 & 0 \end{bmatrix}. \end{aligned} \quad (17)$$

The unit vector $\mathbf{u}_{i,j}^k$ is given by (13) and

$$\mathbf{v}_{i,j}^k = \frac{P_{\mathbf{u}}^\perp (\mathbf{v}_j^k - \mathbf{v}_i^k)}{\|\mathbf{p}_j^k - \mathbf{p}_i^k\|}, \quad (18)$$

with the orthogonal projector

$$P_{\mathbf{u}}^\perp = \mathbb{I}_3 - \mathbf{u}_{i,j}^k (\mathbf{u}_{i,j}^k)^T, \quad (19)$$

see [14]. The observation covariance matrix is

$$\mathbf{R}^k = \text{diag} \left\{ \dots, \sigma_{\rho_{i,j}^k}^2, \sigma_{\dot{\rho}_{i,j}^k}^2, \dots \right\}. \quad (20)$$

3. BAYESIAN CRAMÉR-RAO BOUND

As a limit on the achievable variance, we calculate the recursive Bayesian Cramér-Rao bound for tracking following [15, 16]. We start with the prior Bayesian information matrix (BIM),

$$\mathbf{J}^0 = \text{diag} \left\{ \dots, \sigma_{\mathbf{p}_i^0}^2 \mathbb{I}_3, \sigma_{\mathbf{v}_i^0}^2 \mathbb{I}_3, \sigma_{c\delta_i^0}^2, \sigma_{\dot{c}\delta_i^0}^2, \dots \right\}^{-1}. \quad (21)$$

For the linear process model and nonlinear observation model defined in Sections 2.2 and 2.3, the BIM for consecutive epochs is obtained recursively,

$$\begin{aligned} \mathbf{J}^{k+1} &= (\mathbf{Q}^k + \mathbf{F}^k (\mathbf{J}^k)^{-1} (\mathbf{F}^k)^T)^{-1} \\ &\quad + \mathbf{E}_{\mathbf{x}^{k+1}} \left\{ (\mathbf{H}^{k+1})^T (\mathbf{R}^{k+1})^{-1} \mathbf{H}^{k+1} \right\}, \end{aligned} \quad (22)$$

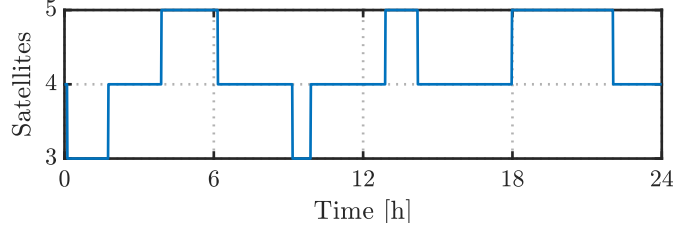


Fig. 2. Number of visible satellites.

see [16]. While (22) is exact, due to the small process noise for the target application, see Section 4.1, we can neglect the expectation operator and evaluate the equation only at the true state [16]. The BCRB for epoch k is then obtained by inverting the BIM,

$$\text{MSE} \{ \mathbf{x}^k \} \geq \text{BCRB} (\mathbf{x}^k) = (\mathbf{J}^k)^{-1}. \quad (23)$$

4. SIMULATION

4.1. Parameters

We assume five Lunar satellites with orbits and signals defined by [4] and time interval between epochs $T = 1$ s. The orbits are simulated using the General Mission Analysis Tool (GMAT) [17], see Fig. 1. As an exemplary location, we have chosen landing site 1 from [18] close to the Lunar south pole with latitude -89.45° , longitude 222.69° . We assume one static user at the landing site and four users uniformly distributed on a circle with radius 1 km moving with 1 m/s on the circle.

Position and velocity of a robotic rover can in general be well predicted using wheel or visual odometry and inertial sensors, thus we have chosen a low velocity noise coefficient $\sigma_{i,v} = 0.001$ m/s^{1.5}. We consider an exemplary space-grade oven-controlled crystal oscillator (OCXO) [19], for which we obtained the clock noise coefficients $\sigma_{i,c1} = 2.52 \cdot 10^{-23}$ s, $\sigma_{i,c2} = 3.03 \cdot 10^{-24}$ s⁻¹ based on the maximum Allan deviation stated in the data sheet.

For a signal transmitted by a Lunar satellite, the error is dominated by the orbit and clock uncertainty of the satellite $\sigma_{\mathbf{p}_j} = 15$ m, $\sigma_{\mathbf{v}_j} = 0.15$ m/s, $\sigma_{c\delta_j} = 10$ m, $\sigma_{\dot{c}\delta_j} = 0.1$ m/s, see [4, 7]. The DLL and FLL noise standard deviations σ_{DLL} and σ_{FLL} are calculated following [20] with the parameters from [4]. For a signal transmitted by another user, the transmitting user is also part of the state space, thus its position and clock errors are considered implicitly. The user range error is dominated by a bias due propagation effects, specifically the two-ray ground reflection [21], which is highly varying depending on distance and terrain. We capture this increased error through a high standard deviation $\sigma_{\rho_u} = 0.5$ m and $\sigma_{\dot{\rho}_u} = 1$ m/s. As prior uncertainty we assume $\sigma_{\mathbf{p}_i^0} = 1000$ m, $\sigma_{\mathbf{v}_i^0} = 10$ m/s, $\sigma_{c\delta_i^0} = 1000$ m, $\sigma_{\dot{c}\delta_i^0} = 100$ m/s.

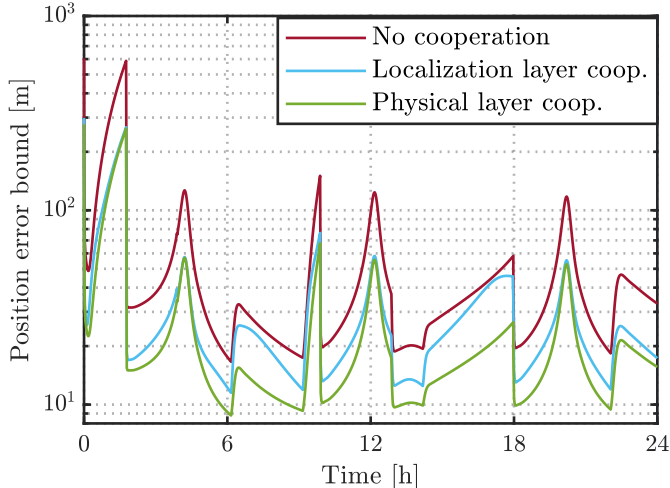


Fig. 3. Three-sigma mean position error bound for five moving users without cooperation, with localization layer cooperation (distance observations) and with physical layer cooperation (pseudorange and Doppler observations).

4.2. Results

Fig. 2 shows the number of visible satellites for the landing site, considering the height of the landing site, a 5° elevation mask and a C/N_0 limit of 30 dB-Hz.

We assume all five users are moving and compare three different cases. First, the users receive only satellite signals and there is no cooperation between users. Second, users cooperate on the localization layer, meaning they can observe noisy distances to their neighbors. Third, users cooperate on the physical layer, meaning the local communication system is driven by the same oscillator as the satellite receiver. Fig. 3 shows the three-sigma mean position error bound $3\sqrt{\frac{1}{|\mathbf{U}|} \sum_{i \in \mathbf{U}} \text{tr}\{\text{BCRB}(\mathbf{p}_i)\}}$. The benefit of cooperation regarding the achievable positioning performance is clearly visible. Furthermore, physical layer cooperation outperforms localization layer cooperation, which highlights the importance of designing the system appropriately.

Now we analyze the case where the user at the landing site is static and the four other users are moving. Fig. 4 shows the comparison of no cooperation to physical layer cooperation for the static user U1 and the moving users U2-U5. As expected, the position BCRB of the static user decreases steadily over time. More important, the moving users benefit considerably from the cooperation. Their position BCRB is a lot less sensitive to the satellite geometry and considerably lower compared to Fig. 3.

Fig. 5 shows the mean position BCRB for a growing number of users. The users are uniformly distributed within a radius of 1 km around the landing site and move with 1 m/s. The plot shows that we do not need a large number of users to benefit from cooperation. In fact, the performance gain per

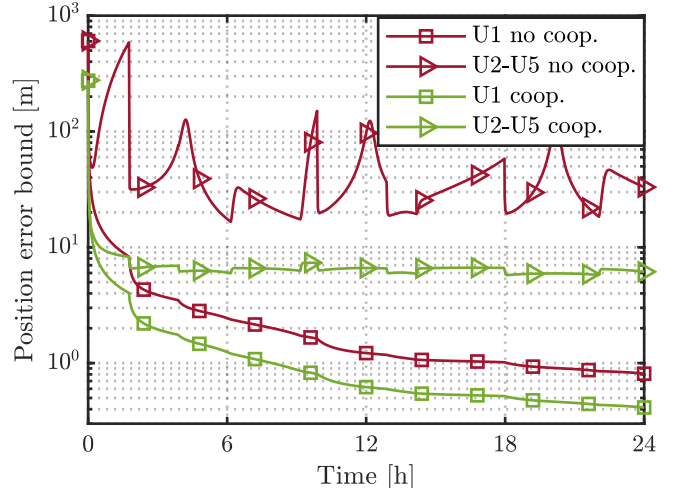


Fig. 4. Three-sigma mean position error bound for static user U1 and mean of moving users U2-U4 without cooperation and with physical layer cooperation.

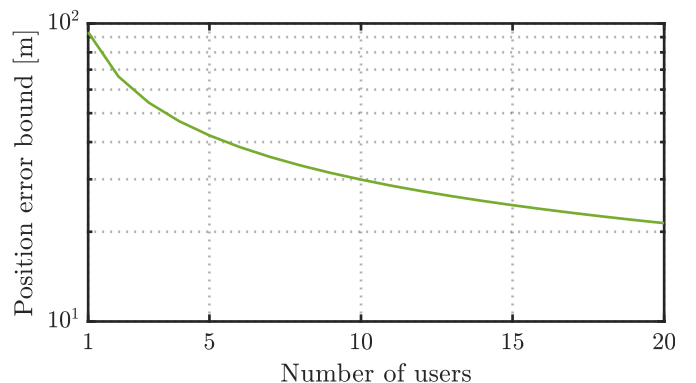


Fig. 5. Three-sigma mean position error bound for varying number of users with physical layer cooperation.

additional user is largest for few users.

5. CONCLUSION

In this paper, we have provided a first analysis of combining Lunar satellite navigation with cooperative navigation on the Lunar surface. We have shown that cooperation considerably improves positioning performance, which is important due to the challenging nature of Lunar PNT with only few available satellites. Specifically, we have shown that physical layer cooperation, where cooperative and satellite navigation systems use the same oscillator, outperforms localization layer cooperation, where only distances between users are observed. Furthermore, cooperating users greatly benefit from a static user. Positioning performance increases with a growing number of users, but the performance gain per additional user is largest for few users.

6. REFERENCES

- [1] International Space Exploration Coordination Group, “The global exploration roadmap,” Jan. 2018.
- [2] Mahesh Anand, “Lunar water: A brief review,” *Earth, Moon, and Planets*, vol. 107, no. 1, pp. 65–73, Dec. 2010.
- [3] Miriam Schönfeldt, Antoine Grenier, Anaïs Delépaut, Richard Swinden, Pietro Giordano, and Javier Ventura-Traveset, “Across the Lunar landscape - exploration with GNSS technology,” *Inside GNSS*, Oct. 2020.
- [4] Antoine Grenier, Pietro Giordano, Lorenzo Bucci, Alexander Cropp, Paolo Zoccarato, Richard Swinden, and Javier Ventura-Traveset, “Positioning and velocity performance levels for a Lunar lander using a dedicated Lunar communication and navigation system,” *NAVIGATION: Journal of the Institute of Navigation*, vol. 69, no. 2, pp. navi.513, June 2022.
- [5] Marco Mangialardo, Maria Manzano Jurado, David Hagan, Pietro Giordano, Paolo Zoccarato, and Javier Ventura-Traveset, “Autonomous navigation for Moon missions: A realistic performance assessment, considering Earth GNSS signals and LCNS constellation,” in *Proc. 10th Workshop Satellite Navigation Technology (NAVITEC)*, Apr. 2022.
- [6] Luciano Musumeci, Fabio DAVIS, João S. Silva, Pedro F. da Silva, and Hugo D. Lopes, “Design of a high sensitivity GNSS receiver for Lunar missions,” *Advances in Space Research*, vol. 57, no. 11, pp. 2285–2313, June 2016.
- [7] Floor Thomas Melman, Paolo Zoccarato, Csilla Orgel, Richard Swinden, Pietro Giordano, and Javier Ventura-Traveset, “LCNS positioning of a Lunar surface rover using a DEM-based altitude constraint,” *Remote Sensing*, vol. 14, no. 16, pp. 3942, Jan. 2022.
- [8] Siwei Zhang, Robert Pöhlmann, Thomas Wiedemann, Armin Dammann, Henk Wymeersch, and Peter Adam Hoehner, “Self-aware swarm navigation in autonomous exploration missions,” *Proceedings of the IEEE*, vol. 108, no. 7, pp. 1168–1195, July 2020.
- [9] R. Michael Buehrer, Henk Wymeersch, and Reza Monir Vaghefi, “Collaborative sensor network localization: Algorithms and practical issues,” *Proceedings of the IEEE*, vol. 106, no. 6, pp. 1089–1114, June 2018.
- [10] Moe Z. Win, Yuan Shen, and Wenhan Dai, “A theoretical foundation of network localization and navigation,” *Proceedings of the IEEE*, vol. 106, no. 7, pp. 1136–1165, July 2018.
- [11] Robert Pöhlmann, Emanuel Staudinger, Siwei Zhang, Fabio Broghammer, Armin Dammann, and Peter A. Hoehner, “Cooperative radio navigation for robotic exploration: Evaluation of a space-analogue mission,” in *Proc. IEEE/ION Position, Location and Navigation Symp. (PLANS)*, Apr. 2023, pp. 372–380.
- [12] Yaakov Bar-Shalom, X. Rong Li, and Thiagalingam Kirubarajan, *Estimation with Applications to Tracking and Navigation: Theory Algorithms and Software*, John Wiley & Sons, 2004.
- [13] Christian Trainotti, Tobias D. Schmidt, and Johann Furthner, “Comparison of clock models in view of clock composition, clock steering and measurement fitting,” in *Proc. 50th Annu. Precise Time and Time Interval Systems and Applications Meeting*, Reston, Virginia, Feb. 2019, pp. 265–283.
- [14] François Vincent, Jordi Vilà-Valls, Olivier Besson, Daniel Medina, and Eric Chaumette, “Doppler-aided positioning in GNSS receivers - A performance analysis,” *Signal Processing*, vol. 176, pp. 107713, Nov. 2020.
- [15] Petr Tichavsky, Carlos H. Muravchik, and Arye Nehorai, “Posterior Cramér-Rao bounds for discrete-time nonlinear filtering,” *IEEE Transactions on Signal Processing*, vol. 46, no. 5, pp. 1386–1396, May 1998.
- [16] Harry L. Van Trees and Kristine L. Bell, Eds., *Bayesian Bounds for Parameter Estimation and Nonlinear Filtering/Tracking*, IEEE Press, Hoboken, NJ, 2007.
- [17] NASA, “General Mission Analysis Tool (GMAT) Version R2022a (GSC-19097-1),” .
- [18] E. Mazarico, G.A. Neumann, D.E. Smith, M.T. Zuber, and M.H. Torrence, “Illumination conditions of the lunar polar regions using LOLA topography,” *Icarus*, vol. 211, no. 2, pp. 1066–1081, Feb. 2011.
- [19] AXTAL, “AXIOM70SL Ultra-Low Phase Noise 10 MHz OCXO with HCMOS output for Space Application (Space COTS version), Rev. 2,” Apr. 2023.
- [20] Elliott D. Kaplan and Christopher J. Hegarty, Eds., *Understanding GPS: Principles and Applications*, Artech House Mobile Communications. Artech House, Boston, Mass., 2 edition, 2006.
- [21] Emanuel Staudinger, Robert Pöhlmann, Armin Dammann, and Siwei Zhang, “Limits on cooperative positioning for a robotic swarm with time of flight ranging over two-ray ground reflection channel,” *Electronics*, vol. 12, no. 9, pp. 2139, Jan. 2023.